

# Stellar haloes of simulated Milky Way-like galaxies: Chemical and kinematic properties

Patricia B. Tissera<sup>1,2</sup>, Cecilia Scannapieco<sup>3</sup>, Timothy C. Beers<sup>4</sup>, Daniela Carollo<sup>5</sup>

<sup>1</sup> *Consejo Nacional de Investigaciones Científicas y Técnicas, CONICET, Argentina.*

<sup>2</sup> *Instituto de Astronomía y Física del Espacio, Casilla de Correos 67, Suc. 28, 1428, Buenos Aires, Argentina.*

<sup>3</sup> *Leibniz-Institut für Astrophysik Potsdam (AIP), An der Sternwarte 16, D-14482 Potsdam, Germany.*

<sup>4</sup> *National Optical Astronomy Observatory, Tucson, 85719, USA.*

<sup>5</sup> *Macquarie University, Dept. Physics & Astronomy, Sydney, 2109 NSW, Australia.*

2 December 2024

## ABSTRACT

We investigate the chemical and kinematic properties of the diffuse stellar haloes of six simulated Milky Way-like galaxies from the Aquarius Project. Binding energy criteria are adopted to define two dynamically distinct stellar populations: the diffuse inner and outer haloes, which comprise different stellar sub-populations with particular chemical and kinematic characteristics. Our simulated inner- and outer-halo stellar populations have received contributions from debris stars (formed in sub-galactic systems while they were outside the virial radius of the main progenitor galaxies) and endo-debris stars (those formed in gas-rich sub-galactic systems inside the dark matter haloes). The inner haloes possess an additional contribution from disc-heated stars in the range  $\sim 3 - 30\%$ , with a mean of  $\sim 20\%$ . Disc-heated stars can exhibit signatures of kinematical support, in particular among the youngest ones. Endo-debris plus disc-heated stars define the so-called *in situ* stellar populations. In both the inner- and outer-halo stellar populations, we detect contributions from stars with moderate to low  $[\alpha/\text{Fe}]$  ratios, mainly associated with the endo-debris or disc-heated sub-populations. The observed abundance gradients in the inner-halo regions are influenced by both the level of chemical enrichment and the relative contributions from each stellar sub-population. Steeper abundance gradients in the inner-halo regions are related to contributions from the disc-heated and endo-debris stars, which tend to be found at lower binding energies than debris stars. In the case of the outer-halo regions, although  $[\text{Fe}/\text{H}]$  gradients are relatively mild, the steeper profiles arise primarily due to contributions from stars formed in more massive satellites, which sink farther into the main halo system, and tend to have higher levels of chemical enrichment and lower energies. Our findings support the existence of (at least) two distinct diffuse stellar halo populations, as suggested by a number of recent observations. Our results also indicate that a comparison of the range of predicted kinematics, abundance gradients, and frequency of  $[\alpha/\text{Fe}]$ -deficient stars with observations of these quantities in the Milky Way, M31, and other large spirals can both provide clues to improve the modelling of baryonic physics, and reveal detailed information about their likely history of formation and evolution.

**Key words:** galaxies: haloes, galaxies: structure, cosmology:theory

## 1 INTRODUCTION

The current cosmological paradigm postulates that large galaxies formed from the hierarchical aggregation of smaller ones (e.g., White & Rees 1978). Within this context, a galaxy such as the Milky Way (MW) is expected to have an assembly path where infall, mergers, and interactions contribute, with their different relative importance influenced by the local environment. Cosmological simulations

are the most suitable tool to describe this complex history of formation, and to confront the adopted cosmological scenario and baryonic sub-grid models with observations. Sophisticated numerical codes have been developed over the past few years, and they are continuously being updated to improve their representation of different physical processes (e.g., Springel 2005; Stinson et al. 2006; Scannapieco et al. 2009; Schaye 2011; Guedes et al. 2011; Brook et al. 2012). In particular, the treatment of chemical evolution within

cosmological codes provides a powerful tool for exploring galaxy formation, and to confront models and observations (e.g., Mosconi et al. 2001; Lia et al. 2002; Governato et al. 2007). In this regard, stellar haloes, such as those of the MW and M31, are valuable laboratories for confronting expectations from cosmological models, since most of their stars are quite old, and were born in the first epochs of galaxy formation. Their chemical abundance patterns, preserved basically unchanged over their long lifetimes, provide a fossil record of the physical characteristics of the interstellar medium at the time and place of their birth (e.g., Bland-Hawthorn & Freeman 2003). We also acknowledge the need to better develop the sets of questions to be posed to models, so that their full utility for exploration of the expected behaviour of actual galaxies can be realized. In this paper, we make a first effort in this direction.

Recent observations provide evidence that the MW halo system comprises at least two overlapping stellar components, an inner-halo population and an outer-halo population, with different metallicities, kinematics, and spatial density profiles (see, e.g., Carollo et al. 2007, 2010; de Jong et al. 2010; Jofré & Weiss 2011; An et al. 2012; Beers et al. 2012; Hattori et al. 2012; Kafle et al. 2012; Kinman et al. 2012). These findings suggest a dual history of halo formation, with contributions from stars accreted from lower-mass sub-galactic systems and those formed *in situ*. Important additional information on the nature of the halo of the MW has begun to emerge from consideration of the chemical abundances of the light and heavy elements. For example, Carollo et al. (2012) have shown that clear differences exist between the frequencies of the so-called carbon-enhanced metal-poor (CEMP) stars that they kinematically associate with the inner- and outer-halo populations. They also present evidence for the existence of a correlation between the frequency of CEMP stars and distance from the Galactic plane, a result which is difficult to understand in the absence of (at least) a dual halo. Roederer (2009) has argued that kinematically separated members of the inner- and outer-halo population exhibit a mean  $[\text{Mg}/\text{Fe}]$  ratio for the outer halo that is lower than that of the inner halo, by about 0.1 dex. He also demonstrated that the star-to-star scatter in  $[\text{Ni}/\text{Fe}]$  and  $[\text{Ba}/\text{Fe}]$  for stars associated with the inner halo is consistently smaller than that of the outer halo. The existence of different stellar populations located within the inner-halo region of the MW has recently emerged from studies of the  $\alpha$ -elements (e.g., Nissen & Schuster 2010; Sheffield et al. 2012). Clearly separable correlations have been shown to exist between  $[\alpha/\text{Fe}]$  and  $[\text{Fe}/\text{H}]$  ('high- $\alpha$ ' and 'low- $\alpha$ ' sequences), as well as with kinematics. Most recently, Schuster et al. (2012) have extended these differences to include ages.

State-of-the-art observations are also providing information on the stellar haloes of nearby galaxies. The nature of the stellar halo of M31 has only recently become feasible to explore in detail, due to large-scale surveys enabled by modern detectors as well as deep Hubble Space Telescope observations (e.g., Sarajedini et al. 2012; Williams et al. 2012). Sarajedini et al. presented evidence that the M31 spheroid possesses a bimodal metallicity distribution, similar in many ways to that suggested by Carollo et al. (2007, 2010) to apply to the MW. In addition, M32 has been reported to exhibit different spheroid populations, with the outer one be-

ing 1.3 Gyr older and  $\sim 0.2$  dex more metal poor than its inner halo (Brown et al. 2007).

From a theoretical point of view, cosmological simulations of galaxy formation within the concordance  $\Lambda$ -CDM model have also made progress in the description of the formation history of stellar haloes. Zolotov et al. (2009) showed a dual history of formation for stellar haloes, with contributions from both accreted sub-galactic systems and *in situ* star formation, the latter principally located in the central regions of the haloes. More recently, similar findings have been reported by Font et al. (2011), McCarthy et al. (2012) and Tissera et al. (2012), through the analysis of stellar haloes in simulated galaxies using a variety of numerical codes and sub-grid physics models. Considering the different approaches used for the baryonic sub-grid models among these cosmological codes, it is noteworthy that they all agree on suggesting a dual formation history for the stellar haloes, in the sense that they are formed by the combination of stars born *in situ* and in accreted sub-galactic systems. This simple way of describing a complex assembly process, which depends strongly on the galaxy evolutionary path, has been successful at illustrating the global picture. To move forward, in this work we aim at studying in more detail the origin of each different stellar populations that form the diffuse haloes in a  $\Lambda$ -CDM scenario.

The results discussed in this paper are related to those reported by Tissera et al. (2012, hereafter, Paper I) who analysed the chemical properties of galaxies formed in eight MW mass-size systems of the Aquarius Project, with different assembly paths within the  $\Lambda$ -CDM scenario Scannapieco et al. (2009). Paper I shows that, although the central regions of these simulated galaxies and their stellar haloes are dominated by very old stars, their chemical properties differ as a consequence of their individual formation histories. The former were dominated by *in situ* star formation, the latter were assembled mainly from small accreted sub-galactic systems. Although the mass scales and time scales involved resulted in different chemical patterns at  $z = 0$ , these simulations successfully reproduced the global chemo-dynamical trends observed in the MW.

Following Paper I, we adopt binding energy criteria defined to dynamically separate two stellar halo populations without any assumptions on the chemical abundances or kinematics of the stars. Hereafter, to clarify the description of our results, the most gravitationally bound stars, dynamically associated with the so-called inner haloes, will be referred to as inner-halo populations (IHPs), while the less bound stars, associated with the so-called outer haloes, will be referred to as outer-halo populations (OHPs). Note that, as the separation of these stellar components is performed on the basis of their binding energy content, the IHPs and OHPs can be spatially superposed. We thus also distinguish these spatial differences by referring to the inner-halo regions (IHRs) and outer-halo regions (OHRs); the relative dominance of the different stellar populations found within these regions naturally differs from one simulated galaxy to the next, depending on its formation history. The properties of the combined IHPs and OHPs, as might be presented to an observer in the IHRs and OHRs, will be discussed in a forthcoming paper.

To understand their history of assembly, we classify the stars in the IHPs and OHPs into three sub-populations ac-

cording to their sites of formation: (1) *debris* stars are formed in separate sub-galactic systems which were later accreted by the progenitor galaxies (i.e. dry mergers as well as the old populations from wet mergers), (2) *disc-heated* stars are formed in a disc-like structure of the progenitor galaxies, then heated up by some violent event, and (3) *endo-debris* stars are those formed in gas-rich sub-galactic systems that survive farther into the dark matter haloes (i.e. wet mergers). In previous works, disc-heated and endo-debris stars have been classified as the *in situ* component. We distinguish them because, at least in our simulations, they exhibit different properties which might help link observations with galaxy formation models. Note that we have cleaned our haloes from bound substructures that could be isolated in density phase. These substructures will be studied in a separate paper.

This paper is organized as follows. In Section 2, we describe the simulations and the main aspects of our chemical-enrichment model. This section also explains the criteria adopted to separate different stellar components. In Section 3, we study the chemical and kinematic properties of the different stellar sub-populations contributing to the IHPs. In Section 4, we discuss the nature of the OHPs. We summarize our findings in Section 5.

## 2 THE SIMULATED MILKY WAY-LIKE SYSTEMS

We analyse a suite of six high-resolution simulations of MW galaxy-sized systems of the original sample from the Aquarius Project, which include the physics of baryons as described by Scannapieco et al. (2009). We first selected six out of the eight cases discussed by Scannapieco et al. (2009), because two haloes experienced important mergers in the recent past, unlike in the MW. The six selected haloes (A, B, C, D, G and H) have surviving discs of different bulge-to-total mass ratios (see Scannapieco et al. 2011, and Paper I).

The target haloes were selected from a cosmological volume consistent with a  $\Lambda$ -CDM cosmogony, with parameters  $\Omega_m = 0.25$ ,  $\Omega_\Lambda = 0.75$ ,  $\sigma_8 = 0.9$ ,  $n_s = 1$  and  $H_0 = 100 h \text{ km s}^{-1} \text{ Mpc}^{-1}$ , and  $h = 0.73$  (see Springel et al. 2008) for further details on the generation of the initial conditions). The simulations were run with a version of GADGET-3 (Springel 2005), which includes a multiphase medium, SN energy feedback, and chemical evolution, as described in Scannapieco et al. (2005, 2006). Maximum gravitational softenings in the range  $\epsilon_G = 0.5 - 1 \text{ kpc } h^{-1}$  were adopted. Virialized structures are identified by requiring the mean overdensity to reach  $\approx 200$  times the cosmological critical density. The simulated haloes have  $\approx 1$  million total particles within the virial radius, and a virial mass in the range  $\approx 5 - 11 \times 10^{11} \text{ M}_\odot h^{-1}$  at  $z = 0$ . Dark matter particles carry masses on the order of  $\approx 10^6 \text{ M}_\odot h^{-1}$ , while, initially, gas particles possess a total mass of  $\approx 2 \times 10^5 \text{ M}_\odot h^{-1}$ . Their characteristic parameters are summarized in Table 1 and Table 2 of Tissera et al. (2010, see also Scannapieco et al. 2009).

### 2.1 The numerical code

The version of GADGET-3 used to run these simulations includes a multiphase model for the gas component, metal-dependent cooling, star formation, and SN feedback, as described in Scannapieco et al. (2005) and Scannapieco et al. (2006). These multiphase and SN-feedback models have been used to successfully reproduce the star-formation activity of galaxies during quiescent and starburst phases, and are able to drive violent mass-loaded galactic winds with a strength reflecting the depth of the potential well (Scannapieco et al. 2006; De Rossi et al. 2010). This physically-motivated thermal SN-feedback scheme does not include any ad hoc mass-scale-dependent parameters, and has no requirement to switch off cooling or provide a dynamical “kick” to other particles. As a consequence, it is particularly well-suited for the study of galaxy formation in a cosmological context.

Our chemical evolution model includes the enrichment by Type II and Type Ia Supernovae (SNII and SNIa, respectively). A Salpeter Initial Mass Function is assumed, with lower and upper mass cut-offs of  $0.1 \text{ M}_\odot$  and  $40 \text{ M}_\odot$ , respectively. We follow 12 different chemical isotopes: H,  $^4\text{He}$ ,  $^{12}\text{C}$ ,  $^{16}\text{O}$ ,  $^{24}\text{Mg}$ ,  $^{28}\text{Si}$ ,  $^{56}\text{Fe}$ ,  $^{14}\text{N}$ ,  $^{20}\text{Ne}$ ,  $^{32}\text{S}$ ,  $^{40}\text{Ca}$ , and  $^{62}\text{Zn}$ . Initially, baryons are in the form of gas with primordial abundance,  $X_{\text{H}} = 0.76$  and  $Y_{\text{He}} = 0.24$ .

SNII are considered to originate from stars more massive than  $8 \text{ M}_\odot$ . Their nucleosynthesis products are adopted from the metal-dependent yields of Woosley & Weaver (1995). The lifetimes of SNII are estimated according to the metal-and-mass-dependent lifetime-fitting formulae of Raiteri et al. (1996). For SNIa, we adopt the W7 model of Thielemann et al. (1993), which assumes that SNIa events originate from CO white dwarf systems in which mass is transferred from the secondary to the primary star until the Chandrasekhar mass is exceeded, and an explosion is triggered. For simplicity, we assume that the lifetime of the progenitor systems are selected at random over the range  $[0.7, 1.1] \text{ Gyr}$ . To calculate the number of SNIa, we adopt an observationally motivated relative ratio of SNII to SNIa rates, as explained by Mosconi et al. (2001).

The ejection of chemical elements is grafted onto the SN-feedback model, so that chemical elements are distributed within the cold and hot gas phases surrounding a given star particle. The fraction of elements going into each phase is regulated by a free parameter,  $\epsilon_c$ , which also determines the amount of SN energy received by each phase. While the injection of energy follows two different paths, depending on the thermodynamical properties of the gas, chemical elements are injected simultaneously with the occurrence of the SN event. All of these simulations were run with  $\epsilon_c = 0.5$ .

### 2.2 The simulated Aquarius galaxies

In order to analyse the chemical properties of the stars, and to relate them to the assembly history of the final galaxy, Paper I defined different dynamical components by using the binding energy ( $E$ ) and angular momentum content along the rotational axis,  $J_z$ . Discs are defined by those particles with  $J_z/J_{z,\text{Emax}} > 0.65$ . The rest of the stellar particles are taken as part of the spheroidal component. Taking into ac-

**Table 1.** Median Abundances of IHPs and OHPs. First column shows the encoding name of the simulations. The percentage of stellar mass, median [Fe/H] and median [O/Fe] for stars identified as disc-heated, endo-debris and debris sub-populations.

Systems	IHPs									OHPs					
	Disc-heated			Endo-debris			Debris			Endo-debris			Debris		
	%	[Fe/H]	[O/Fe]	%	[Fe/H]	[O/Fe]	%	[Fe/H]	[O/Fe]	%	[Fe/H]	[O/Fe]	%	[Fe/H]	[O/Fe]
Aq-A-5	31	-1.11	0.18	41	-1.26	-0.10	25	-1.45	0.35	20	-1.94	0.02	80	-1.42	0.18
Aq-B-5	3	-	-	29	-1.34	0.01	67	-1.22	0.15	12	-1.31	0.02	88	-1.67	0.19
Aq-C-5	24	-0.78	-0.05	32	-1.37	0.01	44	-1.20	0.31	21	-1.90	0.05	79	-1.29	0.12
Aq-D-5	26	-0.90	-0.06	30	-1.28	-0.09	43	-1.02	0.16	24	-1.75	0.02	76	-1.32	0.15
Aq-G-5	35	-0.90	0.00	23	-1.21	0.07	41	-1.00	0.07	5	-1.57	0.02	93	-1.81	0.18
Aq-H-5	18	-0.80	0.02	35	-0.74	-0.14	45	-0.86	0.16	29	-1.16	0.02	71	-1.17	0.10

count their binding energies, stellar particles are classified as belonging to the central spheroid (‘bulge’) or the inner and outer haloes, so that more energetic particles end up in the halo systems while the less energetic particles define the central spheroids. Although the classification of stars belonging to the inner and outer haloes is made on the assumption of a certain binding energy (as explained in Paper I), variations of this limit only weakly affect our results, if these variations are sensible. We also cleaned the stellar haloes of substructure, as defined by the SUBFIND algorithm, so that the analysed stellar haloes correspond to the diffuse components in density space.

As shown in Paper I, the different dynamical components receive contributions from stars formed both *in situ* and in sub-galactic systems that were later accreted into the potential well of the progenitor systems. These sub-galactic systems were either disrupted as soon as they fell into the main potential well, or, if they survived longer, when they were able to reach more central regions. If gas-rich, such systems could have continued their star formation over a prolonged period. New stars formed in this environment would be more chemically enriched by SNIa than older ones, particularly if these sub-galactic systems had bursty star formation histories. Hereafter, we refer to stars formed in such longer-lived gas-rich sub-galactic systems as *endo-debris* stars, and to the stars formed in sub-galactic systems while they were outside of the main halo as *debris* stars. The former are related to the so-called wet mergers, while the latter are associated with the so-called dry mergers (or to the old stellar populations in wet mergers). According to the definition used in Paper I, endo-debris stars, together with disc-heated stars, form the so-called *in situ* component in our simulations – that is, the collection of stars formed inside the progenitor halo. The fractions of each stellar population associated with each dynamical component is different, and varies from system-to-system, depending on their history of assembly.

Paper I also demonstrated that the OHPs are mainly formed from debris stars, along with a small fraction of *in situ* stars. In order to understand the origin of these stars, we followed each of them back in time, and identified the first sub-galactic system that hosted them. We found that most of the stars that were originally classified as *in situ* stars were in fact formed *in between* available snapshots of the simulations, which complicated their detection. From seeking the original gas particles in which they formed, it is clear that most of them were part of small sub-galactic systems. A

negligible fraction of the stars (and their progenitor gas particles) could not be related to any system, but all of them are old, with formation redshift  $z > 5$ . At such high redshifts, our simulations do not possess sufficient resolution to reliably follow the evolution of the smallest clumps, so we include them within the endo-debris populations. Thus, we will hereafter consider that the OHPs are built up mainly by debris stars from accreted sub-galactic systems, out of which a small fraction might correspond to endo-debris stars.

A similar analysis was carried out for the *in situ* stars in the IHPs. We found that these stars included endo-debris sub-populations as well as disc-heated stars. The latter are stars formed in the disc components, but that were heated sufficiently to become part of inner haloes by  $z \sim 0$ , contributing from  $\sim 3\%$  to  $\sim 30\%$  of the IHPs. These fractions are in agreement with the recently reported  $\sim 20\%$  of disc-heated stellar fraction estimated for the MW halo by Sheffield et al. (2012). Endo-debris stars contribute  $\approx 30\%$  of the IHPs, on average, and include a small fraction of stars which could not be identified as belonging to any sub-galactic system (neither could their gaseous progenitors). We also checked for possible contamination of the IHPs from very extended thick-disc populations, by relaxing the condition for particles to be classified as part of the disc components at  $z = 0$ , assuming  $J_z/J_{z,\text{Emax}} > 0.5$ . No significant differences were found.

In the following sections we analyse the chemical and dynamical properties of the IHPs and OHPs, as populated by contributions from the three different sub-populations: debris stars, disc-heated stars, and endo-debris stars. Table 1 summarizes the percentage of stars in each sub-populations and their median abundances. We emphasize that, at any given time (owing to their extended orbits), stars that are members of the IHPs and OHPs can occupy the same spatial regions (both the IHR and the OHR), with different relative fractions at different distances from the centre. We delay the analysis and discussion on this important point, and its consequences, for a forthcoming paper.

### 3 THE DIFFUSE IHPs

As discussed above, our simulated IHPs are complex structures, with contributions from disc-heated stars, as well as from the debris and endo-debris stellar sub-populations. The debris sub-population is the primary contributor, with an average of  $\sim 45\%$  across the six simulated haloes, while the

endo-debris and disc-heated sub-populations each contribute  $\sim 25\%$  to  $\sim 30\%$ , on average.

To better visualize the global differences between the IHPs in our simulated galaxies, Fig. 1 (left panel) shows the Toomre diagram defined by the median LSR velocities, with each of the contributing sub-populations marked. Velocities are normalized to the  $V_{\text{LSR}\odot}$ , defined for each system as the velocity of a test particle on a circular orbit at 8 kpc in the corresponding potential well. As can be seen from inspection of this figure, the debris and endo-debris sub-populations exhibit, on average, little evidence for strong rotation. Typically, disc-heated stars exhibit different kinematics; most are more rotationally supported than the stars in the other two sub-populations. However, there exist an important subset of disc-heated stars that are kinematically cold, and which cannot be distinguished from debris or endo-debris stars. In fact, there is a clear age dependence on the behaviour of the disc-heated stars – old disc-heated stars ( $> 10$  Gyr; open circles) are kinematically colder than the younger stars ( $< 10$  Gyr; filled circles) that exhibit clear signals of rotational support. Note that, in these simulations, young disc-heated stars are nevertheless older than  $\sim 8$  Gyr. In the case of Aq-A-5, a fraction of old disc-heated stars actually exhibit retrograde rotation, illustrating the complexity and diversity of halo assembly in a hierarchical clustering scenario.

Due to the time delay between the corresponding evolution of the progenitor stars of SNII and SNIa, the  $\alpha$ -element-to-iron ratios provide information about the star-formation history of the systems. Figure 1 (middle panel) shows the median  $[\text{O}/\text{Fe}]$  vs  $[\text{Fe}/\text{H}]$  for the IHPs, segregated into the different stellar sub-populations. On average, debris stars are  $\alpha$ -enriched relative to iron. However, we also find a number of stars with low  $[\alpha/\text{Fe}]$  ratios, varying from 7% to 35%, evidencing contributions from SNIa. The fraction of such stars correlates with the mass of the accreted sub-galactic systems, so that the larger fractions are found in IHPs that which formed from more massive systems. The endo-debris and disc-heated sub-populations have a larger fraction of low (or even sub-solar)  $[\alpha/\text{Fe}]$  ratios. The stellar sub-populations also occupy different locations in the  $[\text{Fe}/\text{H}]$  plane. Debris stars are metal poor, and have the smallest contribution from low- $[\alpha/\text{Fe}]$  stars. Endo-debris stars have lower mean  $[\alpha/\text{Fe}]$  ratios. The disc-heated stars tend to exhibit, on average, both higher metallicities and lower  $[\alpha/\text{Fe}]$  ratios compared to the other sub-populations. As expected, this is particularly true for the younger disc-heated stars.

We found that, on average, 55% of the  $\alpha$ -enriched stars in IHPs belong to the debris sub-components, while disc-heated stars and endo-debris stars contribute, individually, on the order of 20 – 25% of the total mass fraction of  $\alpha$ -enriched stars, on average. Observationally, there is evidence for the existence of halo stars with low  $\alpha$ -enrichment (Nissen & Schuster 2010; Sheffield et al. 2012), although their frequency is not yet clearly determined. The endo-debris sub-populations in the IHPs could be associated with the low- $\alpha$  and low  $[\text{Fe}/\text{H}]$  stars classified as the accreted stars by Sheffield et al. (2012). Observations of the  $[\alpha/\text{Fe}]$  abundance ratios for large, unbiased samples of MW halo stars will provide very important constraints on galaxy formation models. According to our present models, such measurements would be a probe of the complex mixture of stellar sub-populations in the inner haloes of large spiral galaxies

such as the MW and M31. Testable predictions of various formation and evolution scenarios could then be made from which models can be revised and improved.

With respect to the mean rotational velocities, the  $\alpha$ -enriched stars followed the same mean trends of their corresponding sub-populations – those belonging to the debris or endo-debris sub-populations exhibit little or no net rotation with respect to the galactic centre in the range  $[-15, 15]$   $\text{km s}^{-1}$ , while those classified as disc-heated stars tend to exhibit clear prograde rotation ( $\sim 50 \text{ km s}^{-1}$ ), particularly the younger stars. The  $\alpha$ -rich stars tend to be 1 – 2 Gyr older than  $\alpha$ -poor stars. A portion of the latter coming from the disc components can be up to 1 Gyr younger.

Figure 2 shows the ages of the IHPs, as a function of binding energy, for the three different stellar sub-components. The debris stars are the oldest, and they span the entire range of total energies. These stars are among the first ones to be formed; as a consequence, they are primarily low metallicity and  $\alpha$ -enriched relative to iron (as can be appreciated from inspection of Fig. 1). The endo-debris stars tend to be slightly younger, and relatively more gravitationally bound. They formed in gas-rich satellites accreted at  $z > 3$ ; 50% of them were formed in sub-galactic systems with dynamical masses smaller than  $10^{8.5} M_{\odot}$ . On average, these stars have a larger fraction of low  $\alpha$ -enrichment when compared to the debris sub-populations. As mentioned before, there are two distinctive regions occupied by disc-heated stars – the most tightly bound stars tend to be older and  $\alpha$ -enriched, while the younger disc-heated stars extend to higher energies. and are more  $\alpha$ -poor.

Our IHPs comprise primarily very old stars, with more than 50% older than 10 Gyrs (a lookback time comparable to redshift  $z \approx 2$ ), while, on average, only  $\sim 5\%$  of them are younger than  $\sim 7.5$  Gyrs ( $z \approx 1$ ). Most of the latter stars are disc heated. As mentioned above, the oldest stars tend to dominate at higher energies, thus the proportion of old and young stars might be expected to vary with galactocentric distance. Observations of stellar populations in galactic haloes at higher redshifts should help to constrain their assembly (Trujillo & Bakos 2012).

### 3.1 $[\text{Fe}/\text{H}]$ profiles of the diffuse IHPs

The different chemical abundances and binding energy distributions of the stellar sub-populations can imprint differences onto their metallicity distribution profiles, which, in turn, provide information on the relative contributions of each of the sub-populations. Previous works have examined the metallicity profiles of their simulated stellar spheroids as a whole (i.e., central spheroids, inner and outer stellar haloes; Font et al. 2011), or looked at the difference between the inner and the outer stellar haloes (Tissera et al. 2012), and reported that these simulations, within the concordance  $\Lambda$ CDM scenario, are able to reproduce metallicity trends similar to those reported by observers for the MW and M31 (see Introduction for a discussion on this point).

Figure 3 shows the  $[\text{Fe}/\text{H}]$  profiles of the disc-heated, endo-debris, and debris stars, as well as the total profiles. The total metallicity profile is clearly a combination of the contributions from each of the sub-populations, the relative importance of which varies from galaxy-to-galaxy. The resulting metallicity profiles depend on both the level of en-

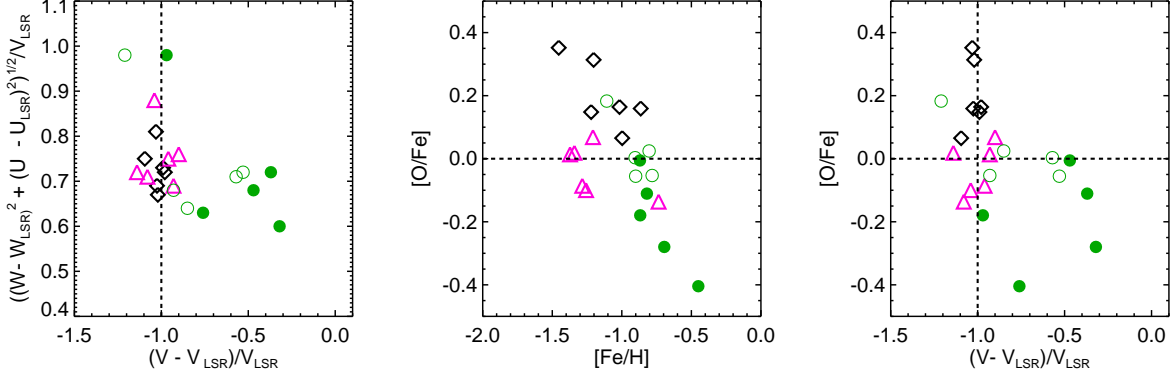


**Figure 1.** Median rotation velocities for stars in the simulations assigned to the IHPs, displayed as the Toomre diagram (left panel),  $[O/Fe]$  versus  $[Fe/H]$  (middle panel), and  $[O/Fe]$  versus rotation velocity for the averaged stellar sub-populations for each of the six simulated haloes, encoded according to: debris stars (diamonds), endo-debris stars (triangles), old disc-heated stars ( $> 10$  Gyr; open circles) and young disc-heated stars ( $8 - 10$  Gyr; filled circles). The vertical dashed lines in the left and right panels denote the limit between prograde and retrograde rotation with respect to the corresponding galactic disc in each simulation. The horizontal dashed lines in the middle and right panels indicate the solar abundance ratio for  $[O/Fe]$ . Note that only 5 symbols are included for the disc-heated stars since Aq-B-5 has a negligible contribution of this sub-population.

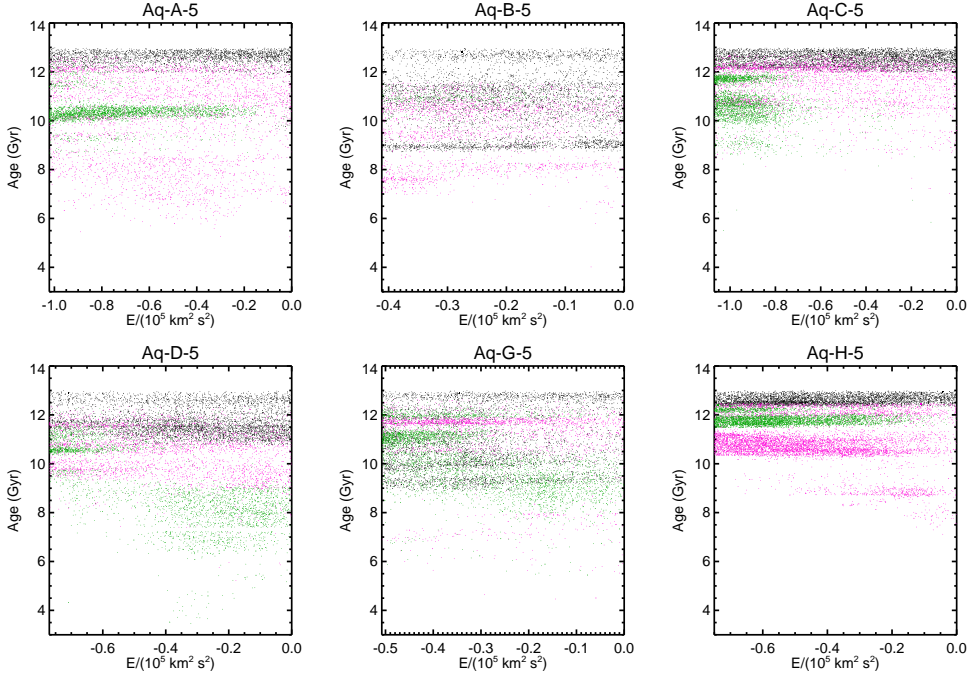


**Figure 2.** Age versus binding energy for the IHPs associated with each of our simulated haloes. Stars are coloured according to their assigned sub-population: debris stars (black), endo-debris stars (magenta) and disc-heated stars (green). For the sake of clarity, we only show  $\sim 30\%$  of the total sample.

richment of the different stellar sub-populations, and their final spatial density distributions. The latter has been included in the corresponding insets of Fig. 3. Hence, although each of these sub-populations may exhibit weak gradients individually, when they are combined, the outcome could be a steeper profile. In fact, in some cases, there exists a sharp transition between the region dominated by the *in situ* sub-populations (i.e., disc-heated plus endo-debris stars) and that dominated by the debris sub-population. In such cases, fitting a simple linear relation might provide

spurious results. Consequently, we prefer to understand the characteristics of the metallicity profiles by analysing the spatial and binding energy distribution of each stellar sub-population. This allows us to assess the role played by each sub-population in shaping the final abundance profiles of the IHPs. The eventual aim is to make use of such profiles (or quantities derived from them) as tools for describing the assembly histories of individual galaxies.

From inspection of Fig. 3, there are three IHRs that exhibit steeper variations of  $[Fe/H]$  with distance than the rest.

In these cases, the *in situ* sub-components (disc-heated stars and/or endo-debris stars) are more centrally concentrated with respect to the debris sub-populations. In the cases with flat  $[\text{Fe}/\text{H}]$  profiles, the three stellar sub-populations are better mixed. This can be seen from the inset of Fig. 3, where we display the spatial distributions of the three different stellar sub-populations in the six analysed haloes. It is clear that Aq-A-5, Aq-C-5, and Aq-G-5 have their *in situ* stars more concentrated toward lower energies (see Fig. 2) and the central regions with respect to the debris stars. Since the disc-heated stars and, in some cases, the endo-debris stars, have higher metallicities in the central regions than debris stars, the abundance profiles are steeper. It can be also seen that the debris stars dominate at larger distances.

According to our simulations, a steep  $[\text{Fe}/\text{H}]$  profile is the result of poorly mixed sub-populations, with significant contributions from either disc-heated stars, endo-debris stars, or both, in the central regions.

## 4 THE DIFFUSE OHPS

The OHPs in our simulated halo systems comprise stars older than  $\sim 11$  Gyr, which are very metal poor and  $\alpha$ -enriched relative to iron. They formed from the accretion of satellite systems, so that most of the stars belong to the debris sub-population. There is a small fraction of stars that originated from an endo-debris sub-population (which were in part classified as *in situ* in Paper I; see Section 2.2).

Regarding the kinematics, we find that most of the OHPs exhibit low net global rotation with respect to their corresponding galactic centres, with mean values in the range  $\langle V_\phi \rangle \sim 20 - 25 \text{ km s}^{-1}$ . One of the six OHPs (Aq-G-5) has a mean  $\langle V_\phi \rangle \sim 7 \text{ km s}^{-1}$ , and another (Aq-C-5) exhibits a retrograde net rotation  $\langle V_\phi \rangle \sim -33 \text{ km s}^{-1}$ . At least in our simulations, the stars are very well-mixed dynamically, so no significant differences in the Toomre diagram could be found between the debris stars and the endo-debris stars, or between the low- and high- $[\alpha/\text{Fe}]$  sub-populations, as can be seen in Fig. 4 (left panel).

The middle panel of Fig. 4 shows the  $[\text{O}/\text{Fe}]$  versus  $[\text{Fe}/\text{H}]$  plane for the debris and endo-debris sub-populations. It is very clear that the endo-debris sub-populations exhibit a larger contribution from low- $[\alpha/\text{Fe}]$  stars, on average. However, there is no trend with rotational velocity, as can be seen from the right panel of Fig. 4. The existence (or absence) of such stars might be tested with observations; their frequency could provide strong constraints on galaxy-formation models and on how the star-formation activity proceeded in small systems at high redshift. Note that most of the stars in the OHPs are located outside the solar neighbourhood; less than  $\approx 10\%$  can be found within this region (Tissera et al. in preparation), thus caution should be taken when compared to available observational surveys.

### 4.1 $[\text{Fe}/\text{H}]$ and $[\text{O}/\text{Fe}]$ Profiles of the OHPS

Previous works have reported the existence of a ‘gradient’ in the metallicity of stars in the simulated halo systems by considering the difference between the so-called IHRs and OHRs. In Paper I, we measured the difference between the

median  $[\text{Fe}/\text{H}]$  of the IHRs and OHRs, finding that simulations were capable of reproducing values similar to those estimated in the MW (Zolotov et al. 2009; Font et al. 2011; McCarthy et al. 2012; Tissera et al. 2012). However, if the analysis is restricted only to the OHRs, one might expect little or no metallicity gradients, at least if the stars from the accreted sub-galactic systems were well-mixed. In Paper I, we found that the median  $[\text{Fe}/\text{H}]$  ( $[\text{O}/\text{Fe}]$ ) of our OHPs are correlated (anti-correlated) with the fractions of stars coming from massive satellites, indicating that some memory of the history of formation may still remain in this component. Below we check on this possibility, assuming that their formation histories are consistent with those predicted by a hierarchical clustering scenario.

Figure 5 shows the median  $[\text{Fe}/\text{H}]$  and  $[\text{O}/\text{Fe}]$  profiles for the OHPs in our six simulated halo systems. For  $[\text{Fe}/\text{H}]$ , there is considerable variation in both the level of enrichment and the predicted slopes with galactocentric distance. We also note that, although this component has been defined to be smooth, the abundance distributions might still reveal their complex assembly histories as shown by  $Jz-E$  in Paper I (see also Helmi & White 2001). This is particularly clear from the  $[\alpha/\text{Fe}]$ -profiles plotted in the lower panel of Fig. 5, where the contributions from the sub-populations with different levels of  $\alpha$ -enrichment as a function of galactocentric radius can be seen.

For the  $[\text{Fe}/\text{H}]$  profiles, a linear regression was fit between  $\sim 20$  kpc and  $\sim 130$  kpc, in order to avoid the central and very outer parts of the distributions, which might be affected by the IHPs and the boundaries of the systems, respectively. Figure 6 shows the slope and zero points, as a function of the fraction of stars formed in more massive sub-galactic systems ( $M > 5 \times 10^9 M_\odot$ ). As expected from the results already discussed in Paper I, the zero point shows a trend indicating higher metallicities in OHPs formed from larger contributions of debris stars acquired from relative more-massive systems. Although the slopes vary from mild to flat, there is a trend with  $F_{\text{massive}}$  such that steeper negative slopes are found in diffuse OHPs formed with significant contributions from relatively higher-mass systems. Massive sub-galactic systems would tend to survive farther into the potential wells, carrying relatively more metal-rich stars and gas available for star formation toward the central regions. The OHPs received a significant contributions of debris from relatively lower-mass satellites will tend to be better-mixed, and exhibit more homogeneous chemical distributions.

In order to better understand the differences in the abundance gradients, we also analysed the ages, spatial distributions, and binding energy distributions of the simulated OHPs. We found that the oldest stars are less metal-enriched, as expected, and they span a larger range of total energy and radial distances. Relatively higher-metallicity stars tend to be more gravitationally bound, and are more centrally concentrated. The outer portions of the OHPs are dominated by high-energy stars, which are also the oldest and the lowest metallicity. To illustrate this, Figure 7 shows the distribution of binding energies for stars in the simulated OHPs, segregated according to  $[\text{Fe}/\text{H}]$ . The two haloes with the flattest metallicity profiles are those that have similar total energy distributions for stars of different  $[\text{Fe}/\text{H}]$  abundances. Those with the steeper slopes possess relatively higher-metallicity stars predominantly at low total energies.

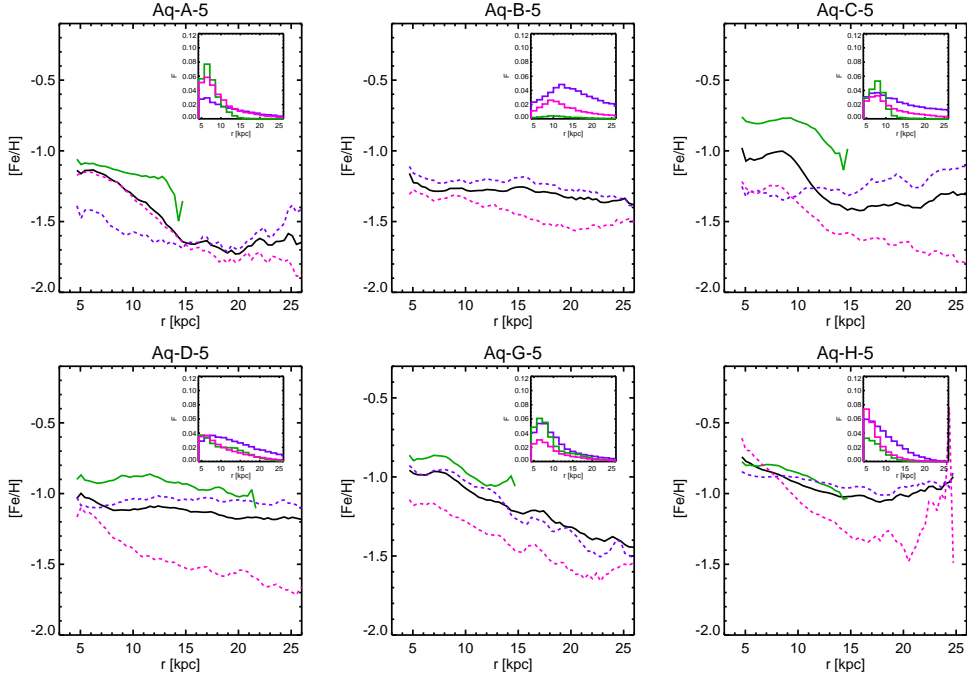


**Figure 3.** Abundance profiles for stellar sub-populations assigned to the IHPs of our six simulated haloes (black lines). The so-called *in situ* component, made up of disc-heated stars (green lines) and endo-debris stars (magenta lines), tends to be located in the central regions and to be dominated by low binding energy particles. The debris stars (violet dashed lines) are more uniformly distributed with distance, and as a consequence, dominate at larger radii. The total abundance profiles are shown in black lines. The inset shows the spatial distribution of the three sub-populations.

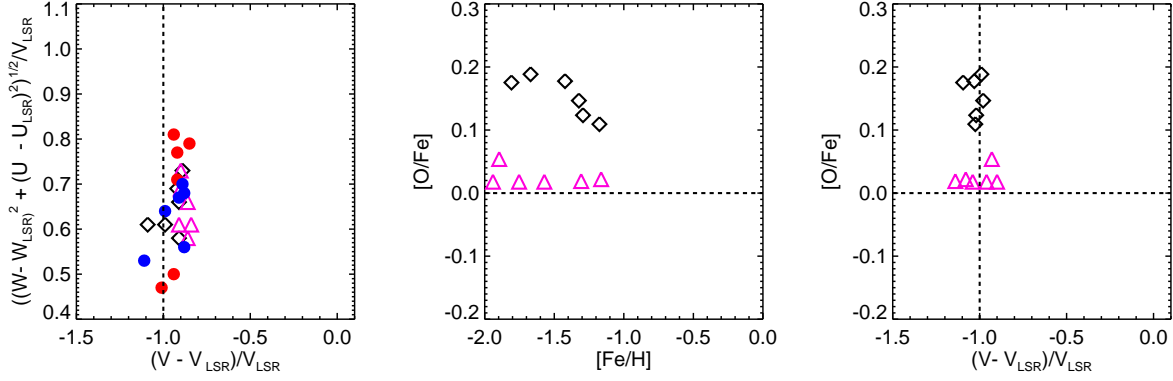


**Figure 4.** Median rotation velocities for stars in the simulations assigned to the OHPs, displayed as the Toomre diagram (left panel),  $[O/Fe]$  versus  $[Fe/H]$  (middle panel), and  $[O/Fe]$  versus rotation velocity for the averaged stellar sub-populations for each of the six simulated haloes, encoded according to: debris stars (diamonds) and endo-debris stars (triangles). For comparison, in the Toomre diagram we included the estimates for the high  $[\alpha/Fe]$  stars (red circles) and low  $[\alpha/Fe]$  stars (magenta circles). The vertical dashed lines in the left and right panels denote the limit between prograde and retrograde rotation with respect to the corresponding galactic disc in each simulation. The horizontal dashed lines in the middle and right panels indicate the solar abundance ratio for  $[O/Fe]$ .

As discussed previously, relatively more-massive satellites contribute higher-metallicity stars. Accordingly, our results indicate that the observed metallicity gradient in the diffuse OHR of a galaxy such as the MW can provide clues about the mass distributions of the satellites that contributed to its formation.

## 5 CONCLUSIONS

We have analysed a suite of six MW mass-sized systems, simulated within  $\Lambda$ CDM using a version of P-GADGET3 that includes a prescription for self-consistent SN feedback. This scheme allows us to follow the chemo-dynamical evolution of baryons as they are assembled into galaxies. Our simulated diffuse stellar haloes can be described as assembled from two primary stellar sub-populations, those formed in originally separate sub-galactic systems, having a dis-



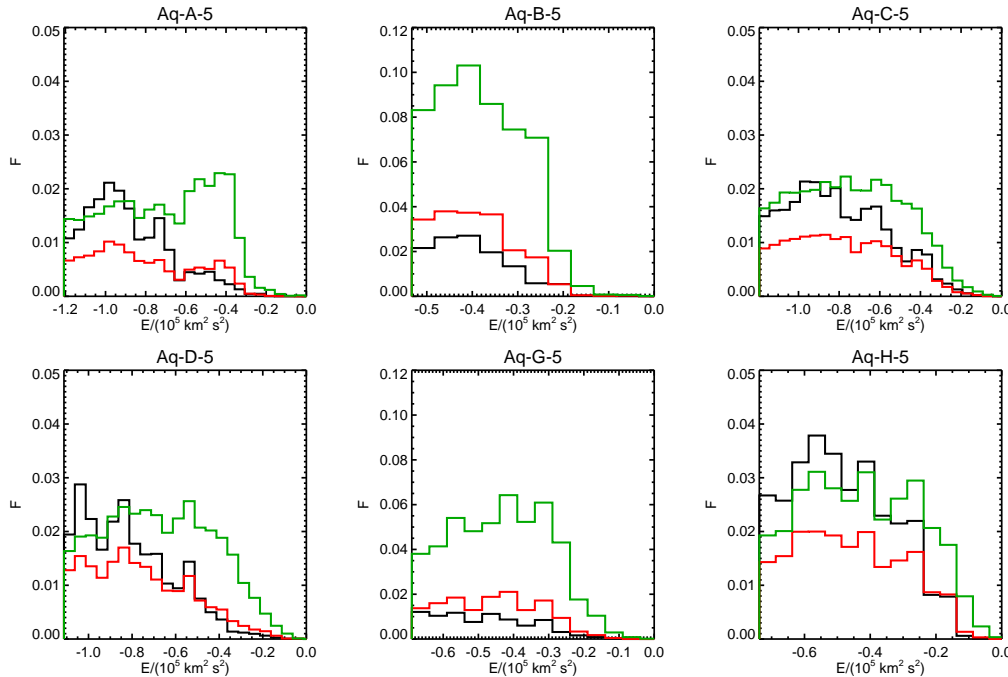


**Figure 7.** Distribution of binding energy,  $E$ , for stars in the diffuse OHPs, divided according to their  $[\text{Fe}/\text{H}]$  abundances:  $[\text{Fe}/\text{H}] > -1$  (black lines),  $-1.5 < [\text{Fe}/\text{H}] < -1$  (magenta lines) and  $[\text{Fe}/\text{H}] < -1.5$  (green lines). Aq-A-5 and A-D-5 have steeper metallicity gradients than Aq-C-5 and A-G-5.

tribution of masses, and those acquired from heated disc-component stars of the main galaxy. We distinguish two types of accreted stars: debris stars, defined as those formed in sub-galactic systems outside the main dark matter halo, and later accreted, donating stars primary to the OHPs but as well as to IHPs, and, endo-debris stars, formed in gas-rich sub-galactic systems which were disrupted farther into the global potential well, contributing stars primarily to the IHPs, and to a lesser degree, to the OHPs. These sub-populations are distinguished from one another as they exhibit, on average, stars of different chemical abundances, ages, kinematics, and binding energies. The relative fractions of debris stars and endo-debris stars provides clues to the mass distribution (and relative number) of the sub-galactic systems that contribute to form the stellar haloes. These results have clear implications for observational studies that attempt to identify different populations in the MW and other galaxies (e.g. Carollo et al. 2010, 2012; Sheffield et al. 2012).

#### Summary of the main results:

The simulated IHPs possess three clear stellar sub-populations – the debris stars, the endo-debris stars, and the disc-heated stars. Debris stars are  $\alpha$ -enhanced relative to iron, low metallicity, and are on average, dynamically cold. Endo-debris stars exhibit lower  $\alpha$ -enhancement than debris ones, on average. Endo-debris stars could be associated with the stars observed and classified by Sheffield et al. (2012) as accreted stars. In our simulations endo-debris stars exhibit larger velocity dispersions, on average, than the disc-heated stars. Disc-heated stars are less  $\alpha$ -enhanced and more metal-rich compared to the endo-debris stars, with characteristics that depend on their ages. Disc-heated stars with ages greater than  $\sim 10$  Gyr are generally kinematically cold,

while those with ages in the range  $\sim 8 - 10$  Gyr are rotationally supported and exhibit solar to sub-solar  $[\alpha/\text{Fe}]$  ratios. Although it is feasible, on average, to distinguish these different components by comparing their chemical abundances and kinematic properties, there exists considerable overlap between these sub-populations.

The simulated IHPs exhibit metallicity gradients, the strength of which are determined by the relative fractions of the three sub-populations that contributed to their formation. While the endo-debris and disc-heated stars dominate in the central parts of IHRs (within  $\approx 20$  kpc), the debris stars dominate in the outer parts of the IHRs. Hence, the relative contributions of the different sub-populations can conspire to produce steeper metallicity gradients than those exhibit by each sub-populations separately.

The simulated OHPs are primarily comprised of debris stars that formed in accreted sub-galactic systems. The relatively less-massive systems are easily disrupted, while the relatively more-massive ones are able to survive farther into the global potential well of the system before being disrupted. As a consequence, although stars of the OHPs are generally of very low metallicity, the relatively more metal-rich ones tend to be more centrally concentrated. The relative distribution of debris stars from these different accreted sub-galactic systems can result in a genuine metallicity gradient within the OHRs, which although weak, can be used to constrain the assembly history of the OHPs. The  $[\alpha/\text{Fe}]$  ratios exhibit a heterogeneous distribution from simulated galaxy-to-galaxy, reflecting the mixture of contributions from accreted galactic systems with different star-formation histories. A future comparison between the frequency of low- $[\alpha/\text{Fe}]$  stars in the haloes can provide clues on the history of formation and the masses of the ac-

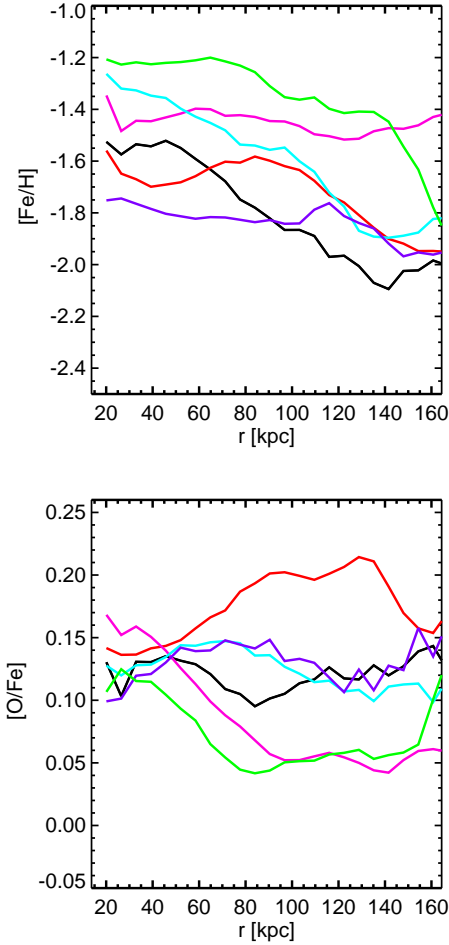


**Figure 5.** Median abundance profiles of  $[\text{Fe}/\text{H}]$  (upper panel) and  $[\text{O}/\text{Fe}]$  (lower panel) for stars in the diffuse OHPs of our six simulated galaxies: Aq-A-5 (black), Aq-B-5 (red), Aq-C-5 (magenta), Aq-D-5 (cyan), Aq-G-5 (green), and Aq-H-5 (violet). See text for discussion.

creted systems, as well as on the validity of current chemical-enrichment schemes.

In this paper, we have studied the IHPs and OHPs as separate sub-populations in relation to their assembly histories in a cosmological context. The properties of the combined IHPs and OHPs will be discussed in a forthcoming paper, which considers comparisons of the nature of the observed stellar populations in the MW, M31, and other nearby galaxies with predictions from the simulations.

## ACKNOWLEDGMENTS

We thank Simon D.M. White for useful comments and suggestions. This work was partially funded by L’Oreal-Unesco-Conicet Award for Women in Science, PICT Max Planck 245 (2006) of the Ministry of Science and Technology (Argentina), and the Cosmocomp and Lacegal Networks of FP7 Programme of the European Community. TCB acknowledges partial funding from grants PHY 02-16783 and PHY 08-22648: Physics Frontier Center / Joint Institute for Nu-

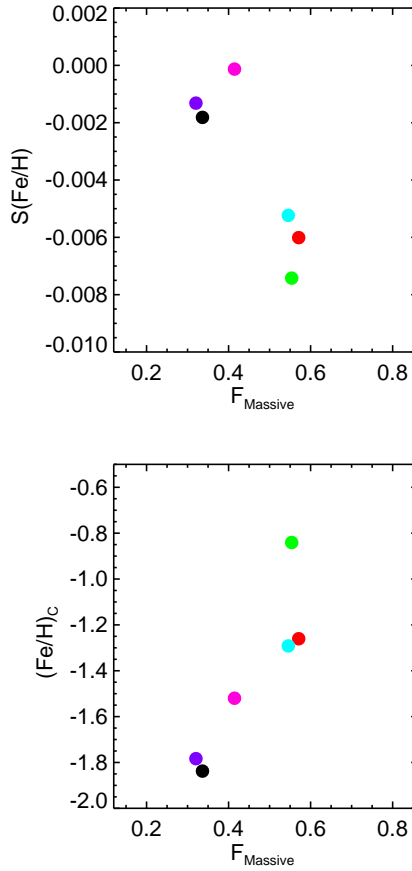


**Figure 6.** Slopes (upper panel) and zero points (lower panel) of linear regressions fit to the  $[\text{Fe}/\text{H}]$  profiles versus the fraction of stars in the diffuse OHPs formed in satellites more massive than  $5 \times 10^9 M_\odot h^{-1}$ . See Fig. refgradhaloe for colour coding of the simulated galaxies.

clear Astrophysics (JINA), awarded by the U.S. National Science Foundation.

## REFERENCES

- An D., Beers T. C., Johnson J. A., Pinsonneault M. H., Lee Y. S., Bovy J., Ivezić Ž., Carollo D., Newby M., 2012, ArXiv e-prints
- Beers T. C., Carollo D., Ivezić Ž., An D., Chiba M., Norris J. E., Freeman K. C., Lee Y. S., Munn J. A., Re Fiorentin P., Sivarani T., Wilhelm R., Yanny B., York D. G., 2012, ApJ, 746, 34
- Bland-Hawthorn J., Freeman K. C., 2003, in E. Perez, R. M. Gonzalez Delgado, & G. Tenorio-Tagle ed., Star Formation Through Time Vol. 297 of Astronomical Society of the Pacific Conference Series, Unravelling the Epoch of Dissipation. pp 457–+
- Brook C. B., Stinson G. S., Gibson B. K., Kawata D., House E. L., Miranda M. S., Macciò A. V., Pilkington K., Roškar R., Wadsley J., Quinn T. R., 2012, MNRAS, 426, 690

- Brown T. M., Smith E., Ferguson H. C., Guhathakurta P., Kalirai J. S., Rich R. M., Renzini A., Sweigart A. V., Reitzel D., Gilbert K. M., Geha M., 2007, *ApJL*, 658, L95
- Carollo D., Beers T. C., Bovy J., Sivarani T., Norris J. E., Freeman K. C., Aoki W., Lee Y. S., Kennedy C. R., 2012, *ApJ*, 744, 195
- Carollo D., Beers T. C., Chiba M., Norris J. E., Freeman K. C., Lee Y. S., Ivezić Ž., Rockosi C. M., Yanny B., 2010, *ApJ*, 712, 692
- Carollo D., Beers T. C., Lee Y. S., Chiba M., Norris J. E., Wilhelm R., Sivarani T., Marsteller B., Munn J. A., Bailer-Jones C. A. L., Fiorentin P. R., York D. G., 2007, *Nature*, 450, 1020
- de Jong J. T. A., Yanny B., Rix H.-W., Dolphin A. E., Martin N. F., Beers T. C., 2010, *ApJ*, 714, 663
- De Rossi M. E., Tissera P. B., Pedrosa S. E., 2010, *ArXiv e-prints*
- Font A. S., Benson A. J., Bower R. G., Frenk C. S., Cooper A., De Lucia G., Helly J. C., Helmi A., Li Y.-S., McCarthy I. G., Navarro J. F., Springel V., Starkenburg E., Wang J., White S. D. M., 2011, *MNRAS*, 417, 1260
- Governato F., Willman B., Mayer L., Brooks A., Stinson G., Valenzuela O., Wadsley J., Quinn T., 2007, *MNRAS*, 374, 1479
- Guedes J., Callegari S., Madau P., Mayer L., 2011, *ApJ*, 742, 76
- Hattori K., Yoshii Y., Beers T. C., Carollo D., Lee Y. S., 2012, *ArXiv e-prints*
- Helmi A., White S. D. M., 2001, *MNRAS*, 323, 529
- Jofré P., Weiss A., 2011, *A&A*, 533, A59
- Kafle P. R., Sharma S., Lewis G. F., Bland-Hawthorn J., 2012, *ArXiv e-prints*
- Kinman T. D., Cacciari C., Bragaglia A., Smart R., Spagna A., 2012, *MNRAS*, 422, 2116
- Lia C., Portinari L., Carraro G., 2002, *MNRAS*, 330, 821
- McCarthy I. G., Font A. S., Crain R. A., Deason A. J., Schaye J., Theuns T., 2012, *MNRAS*, 420, 2245
- Mosconi M. B., Tissera P. B., Lambas D. G., Cora S. A., 2001, *MNRAS*, 325, 34
- Nissen P. E., Schuster W. J., 2010, *A&A*, 511, L10
- Raiteri C. M., Villata M., Navarro J. F., 1996, *A&A*, 315, 105
- Roederer I. U., 2009, *AJ*, 137, 272
- Sarajedini A., Yang S.-C., Monachesi A., Lauer T. R., Trager S. C., 2012, *MNRAS*, 425, 1459
- Scannapieco C., Tissera P. B., White S. D. M., Springel V., 2005, *MNRAS*, 364, 552
- Scannapieco C., Tissera P. B., White S. D. M., Springel V., 2006, *MNRAS*, 371, 1125
- Scannapieco C., White S. D. M., Springel V., Tissera P. B., 2009, *MNRAS*, 396, 696
- Scannapieco C., White S. D. M., Springel V., Tissera P. B., 2011, *MNRAS*, 417, 154
- Schaye J., 2011, in *Galaxy Formation SPH simulations of the formation and evolution of galaxies*
- Schuster W. J., Moreno E., Nissen P. E., Pichardo B., 2012, *A&A*, 538, A21
- Sheffield A. A., Majewski S. R., Johnston K. V., Cunha K., Smith V. V., Cheung A. M., Hampton C. M., David T. J., Wagner-Kaiser R., Johnson M. C., Kaplan E., Miller J., Patterson R. J., 2012, *ArXiv e-prints*
- Springel V., 2005, *MNRAS*, 364, 1105
- Springel V., Wang J., Vogelsberger M., Ludlow A., Jenkins A., Helmi A., Navarro J. F., Frenk C. S., White S. D. M., 2008, *MNRAS*, 391, 1685
- Stinson G., Seth A., Katz N., Wadsley J., Governato F., Quinn T., 2006, *MNRAS*, 373, 1074
- Thielemann F., Nomoto K., Hashimoto M., 1993, in N. Prantzos, E. Vangioni-Flam, & M. Casse ed., *Origin and Evolution of the Elements Explosive nucleosynthesis in supernovae.* pp 297–309
- Tissera P. B., White S. D. M., Pedrosa S., Scannapieco C., 2010, *MNRAS*, 406, 922
- Tissera P. B., White S. D. M., Scannapieco C., 2012, *MNRAS*, 420, 255
- Trujillo I., Bakos J., 2012, *ArXiv e-prints*
- White S. D. M., Rees M. J., 1978, *MNRAS*, 183, 341
- Williams B. F., Dalcanton J. J., Bell E. F., Gilbert K. M., Guhathakurta P., Lauer T. R., Seth A. C., Kalirai J. S., Rosenfield P., Girardi L., 2012, *ArXiv e-prints*
- Woosley S. E., Weaver T. A., 1995, *ApJS*, 101, 181
- Zolotov A., Willman B., Brooks A. M., Governato F., Brook C. B., Hogg D. W., Quinn T., Stinson G., 2009, *ApJ*, 702, 1058